Journal of Molecular Catalysis B: Enzymatic 69 (2011) 120–126

Contents lists available at ScienceDirect

Journal of Molecular Catalysis B: Enzymatic

journal homepage: www.elsevier.com/locate/molcatb

Activity and stability comparison of immobilized NADH oxidase on multi-walled carbon nanotubes, carbon nanospheres, and single-walled carbon nanotubes

Liang Wang, Rong Xu, Yuan Chen, Rongrong Jiang*

School of Chemical & Biomedical Engineering, Nanyang Technological University, 62 Nanyang Drive, Singapore 637459, Singapore

ARTICLE INFO

Article history:
Received 1 October 2010
Received in revised form 10 January 2011
Accepted 10 January 2011
Available online 15 January 2011

Keywords:
NADH oxidase
Multi-walled carbon nanotubes
Carbon nanospheres
Enzyme immobilization

ABSTRACT

Nanomaterials have been studied widely as the supporting materials for enzyme immobilization because in theory, they can provide low diffusion resistance and high surface/volume ratio. Common immobilization methods, such as physical adsorption, covalent binding, crosslinking, and encapsulation, often cause problems in enzyme leaching, 3D structure change and strong mass transfer resistance. We have previously demonstrated a site-specific enzyme immobilization method, which is based on the specific interaction between a His-tagged enzyme and functionalized single-walled carbon nanotubes (SWCNTs), that can overcome the foresaid constraints. In this work, we broadened the use of this immobilization approach by applying it on other nanomaterials, including multi-walled carbon nanotubes and carbon nanospheres. Both supporting materials were modified with N_α,N_α-bis(carboxymethyl)-L-lysine hydrate prior to enzyme immobilization. The resulting nanomaterial–enzyme conjugates could maintain 78–87% of the native enzyme activity and showed significantly better stability than the free enzyme. When compared with the SWCNT–enzyme conjugate, we found that the size variance among these supporting nanomaterials may affect factors such as surface curvature, surface coverage and particle mobility, which in turn results in differences in the activity and stability among these immobilized biocatalysts.

1. Introduction

Nanotechnology-inspired immobilized enzyme systems have attracted a lot of attention in recent years and have been used in various areas including biocatalysis [1], biofuel cell fabrication [2], and biosensor preparation [3]. Theoretically, nanomaterials can provide the upper limit in the key factors that determine the efficiency of biocatalysts, including surface area/volume ratios, mass transfer resistance, and enzyme loading capacity [4]. Moreover, enzyme unfolding is also limited as nanomaterials can confine enzyme molecule into a space of comparable size [5]. Nevertheless, common immobilization methods, including physical adsorption [6], covalent binding [7], entrapment [8] and encapsulation [9], often face constraints in enzyme leaching [10], changes in 3D structure of enzyme [11], and mass transfer resistance [12]. In order to overcome the foresaid limitations, we have developed an effective immobilization method based on the specific interaction between His-tagged enzyme and functionalized single-walled carbon nanotubes (SWCNTs) previously [13]. The resulting SWCNT–enzyme conjugates demonstrated excellent activity retention (>90%) and stability improvement.

Here in this work, we intended to employ the same immobilization procedure on other supporting nanomaterials, such as multi-walled carbon nanotubes (MWCNTs) and carbon nanospheres (CNSs), in order to test the applicability of this method. We have used the same enzyme, NADH oxidase (NOX) from *Bacillus cereus* (*B. cereus*), as in our previous work to facilitate the comparison among the different supporting materials. Many enzymes involved in biological redox reactions require nicotinamide cofactors NAD(P)H/NAD(P)$^+$, such as L-glutamate dehydrogenase [14], L-amino acid dehydrogenase [15], and carbonyl reductase [16]. Because of the high cost of NAD(P)H/NAD(P)$^+$, in situ cofactor regeneration system is often employed during industrial synthesis [17,18]. NOX, which can convert oxygen to either hydrogen peroxide or water, is an excellent NAD$^+$-regenerating enzyme [19,20]. We chose MWCNTs as our supporting materials since MWCNTs are structurally similar to SWCNTs, but their diameters can range from a few nanometers to dozens of nanometers. Compared to SWCNTs, MWCNTs are commercially available at relative lower price, which makes it more feasible for industrial applications [21]. The other supporting materials tested in this study are CNSs. CNSs have substantially larger particle size than MWCNTs and can be easily prepared in large scale from the hydrothermal treatment of glucose solutions with low cost [22,23]. The as-prepared CNSs with diameter between 200 and 800 nm possess abundant surface functional groups such as –OH and –COOH that enable further chemical modifications [22,24].

* Corresponding author. Tel.: +65 65141055; fax: +65 67947553.
E-mail address: rrjiang@ntu.edu.sg (R. Jiang).

1381-1177/$ – see front matter © 2011 Elsevier B.V. All rights reserved.
doi:10.1016/j.molcatb.2011.01.005

In the present study, we modified both MWCNTs and CNSs with N_α,N_α-bis(carboxymethyl)-L-lysine hydrate (ANTA) as described before [13,25]. The His-tagged NOX enzyme was immobilized onto MWCNTs and CNSs via the specific interaction between the His-tag and the Co^{2+} terminated nitrilotriacetate groups present on the supporting materials. Through comparing the various tested nanomaterials in terms of activity, storage stability, thermal stability, and operational stability after enzyme immobilization, we aimed to reveal the relationship between the characteristics of the supporting materials and the activity/stability of the immobilized enzyme.

2. Materials and methods

2.1. Materials

Bradford reagent, cobalt (II) chloride, N_α,N_α-bis(carboxymethyl)-L-lysine hydrate (ANTA), nitric acid, tryptone, 1-ethyl-3-[3′-(dimethylamino)propyl]carbodiimide (EDC), sulfuric acid, N-hydroxysuccinimide (NHS), N-(2-hydroxyethyl)piperazine-N′-(2-ethanesulfonic acid) (HEPES), ampicillin sodium salt, kanamycin sulfate, potassium phosphate dibasic, potassium phosphate monobasic, isopropyl β-D-thiogalactopyranoside (IPTG), potassium bromide and sodium chloride were purchased from Sigma–Aldrich (Singapore). Dithiothreitol (DTT), β-nicotinamide adenine dinucleotide, reduced dipotassium salt (NADH), flavin adenine dinucleotide (FAD), urea, calcium chloride, rubidium chloride, manganese chloride tetrahydrate, and yeast extract were purchased from Merck (Singapore). FloTube™ 9000 multi-walled carbon nanotubes were from CNano Technology Ltd. (China, D_{MWCNT}: 10–20 nm, surface area: 280 m^2/g). CNSs were synthesized according to a previously reported protocol [23]. In brief, 42 ml of an aqueous solution of glucose (0.48 mM) was prepared and transferred to a sealed Teflon-lined stainless steel autoclave with a volume capacity of 53 ml. The solution was raised to 180 °C and kept at this temperature for 8 h. The black-brown precipitates were washed by ethanol and deionized water for several times before being dried at 60 °C for 6 h.

2.2. Cloning, overexpression and purification

The detailed cloning, overexpression and purification process was described in our former publication [13]. In short, *E. coli* BL21 (DE3) containing pET30b(+)-nox recombinant plasmid was cultured in Luria–Bertani (LB) broth containing 30 μg/ml kanamycin at 200 rpm, 37 °C. Protein over-expression was induced by adding 200 μM IPTG when OD at 600 nm reached 0.6–0.8. After cell lysis by sonication, NOX was purified and desalted by immobilized metal affinity chromatography (IMAC; Gravatrap Ni^{2+} column, GE Healthcare, Singapore) and PD-10 desalting column (GE Healthcare, Singapore). Protein purity was checked by sodium dodecyl sulfate-polyacrylamide gel electrophoresis (SDS-PAGE) and its concentration was measured by a Biophotometer (Eppendorf) after 5-min incubation with Bradford Reagent.

2.3. MWCNs and CNSs modifications

Carboxylic acid groups were formed on MWCNTs following a previously reported protocol [26]. MWCNTs were first treated with acid mixture (HNO_3/H_2SO_4 = 1:3, v/v) in a water-bath sonicator at 40 °C for 3 h. The MWCNT suspension was then filtered through a 0.2-μm nylon membrane and washed by 20 mM, pH 7.5 HEPES buffer. The MWCNT–COOH was finally suspended in HEPES buffer. Acid treatment on CNSs is unnecessary due to carboxylic acid groups already present on their surfaces.

MWCNT–COOH, dispersed in 25-ml HEPES buffer, was first activated by 50 mM NHS and 20 mM EDC to form MWCNT–NHS ester complex. ANTA was dissolved in HEPES with excessive $CoCl_2$ to form ANTA–Co^{2+}. Excessive Co^{2+} was precipitated by NaOH and $Co(OH)_2$ was removed by centrifugation at 5000 × *g* for 10 min. The supernatant containing ANTA–Co^{2+} was added to MWCNT–NHS ester to produce MWCNT–ANTA–Co^{2+} complex. The complex was filtered, washed extensively and stored in 20 mM, pH 7.5 HEPES buffer. A similar procedure was performed to functionalize CNSs to obtain complex CNS–ANTA–Co^{2+}.

2.4. MWCNTs and CNSs characterization

The functionalized samples of MWCNT and CNS at different modification stages, as well as the untreated samples, were all characterized by Fourier transformed infrared spectroscopy (FTIR). MWCNTs and CNSs were collected by filtering MWCNTs dispersions with a 0.2-μm nylon membrane, and centrifuging CNSs samples at 12,000 × *g*, respectively. Both samples were dried in a 100 °C oven. The dried samples were mixed with KBr powder, and pressed into thin films for FTIR measurement (FTS 3100, DIGILAB, USA). The IR spectra were averaged over 96 scans from 1000 to 4000 cm^{-1}. The spectra were blank subtracted and the baseline was corrected by Revolution 4.0 Pro software.

2.5. Enzyme immobilization

MWCNT/CNS–ANTA–Co^{2+} complex were incubated with cell lysate at 4 °C overnight. The resulting MWCNT/CNS–ANTA–Co^{2+}–NOX conjugates (MWCNT/CNS–NOX) were collected by centrifugation and washed with 20 mM, pH 7.4 HEPES containing 20 mM imidazole for three times. MWCNT/CNS–NOX were then suspended in 20 mM, pH 7.5 HEPES. In order to measure enzyme loading capacity, free NOX was eluted off MWCNTs and CNSs with 20 mM, pH7.4 HEPES buffer containing 500 mM NaCl and 500 mM imidazole, respectively, and the protein concentrations were measured using Bradford assay.

2.6. Conjugate activity assay

The activity of both MWCNT–NOX and CNS–NOX was measured by monitoring the decrease of NADH absorbance at 340 nm (ε: 6220 $M^{-1}cm^{-1}$) using a DU-800 spectrophotometer (Beckman Coulter, Singapore). The standard conditions were set as follows: 20 μM FAD (MWCNT–NOX)/44 μM FAD (CNS–NOX) in air-saturated 50 mM, pH 7.0 PPB with 200 μM NADH at 30 °C. Both K_M and V_{max} values were determined under standard conditions with NADH concentration varying from 0 to 400 μM.

2.7. Enzyme stability measurement

2.7.1. Effect of temperature

The effect of temperature was investigated by changing reaction temperature between 20 and 90 °C. The activity of the immobilized enzyme was measured under standard conditions. The relative activity of MWCNT–NOX and CNS–NOX was calculated by assigning their maximum activity at optimum temperature as 100%, respectively.

2.7.2. Storage stability

The storage stability of both MWCNT–NOX and CNS–NOX was investigated at 4 °C. The activity of MWCNT–NOX and CNS–NOX

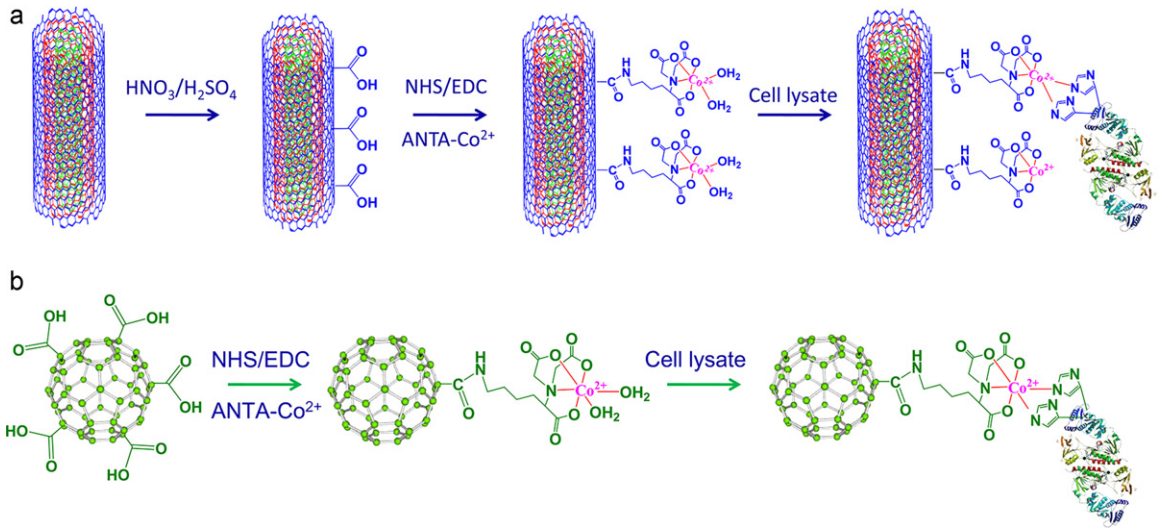

Fig. 1. Scheme of specific immobilization of NADH oxidase (*B. cereus*) on functionalized (a) MWCNTs and (b) CNSs.

was measured at regular time interval under standard conditions, respectively.

2.7.3. Reusability

The reusability of MWCNT–NOX and CNS–NOX was measured by their residual activity under standard conditions. After each reaction, MWCNT–NOX and CNS–NOX were recovered by centrifugation and washed with 20 mM, pH 7.5 HEPES for three times.

2.8. Enzyme deactivation assay

The deactivation of free NOX, SWCNT–NOX, MWCNT–NOX and CNS–NOX was assessed at 50 °C and 90 °C in 50 mM, pH 7.0 PPB, 50 μM FAD, respectively. Residual activity of each sample was determined with 200 μM NADH and calculated by the percentage of the residual enzyme activity to its initial activity.

2.9. Total turnover number measurement

MWCNT–NOX or CNS–NOX was added to the air-saturated 50 mM, pH 7.0 PPB buffer with or without 5 mM DTT at 30 °C. NADH was added until the enzyme could no longer react [19,20].

3. Results and discussion

3.1. MWCNT–NOX and CNS–NOX

The schemes of enzyme immobilization on MWCNTs and CNSs are illustrated in Fig. 1a and b, respectively. We functionalized both MWCNTs and CNSs surface with Co^{2+} terminated nitrilotriacetate groups that would allow the binding of His-tagged NADH oxidase. Pristine MWCNTs were treated with the acid mixture of HNO_3 and H_2SO_4 first, and the activated MWCNTs and CNSs were then amidated by N-hydroxysuccinimide

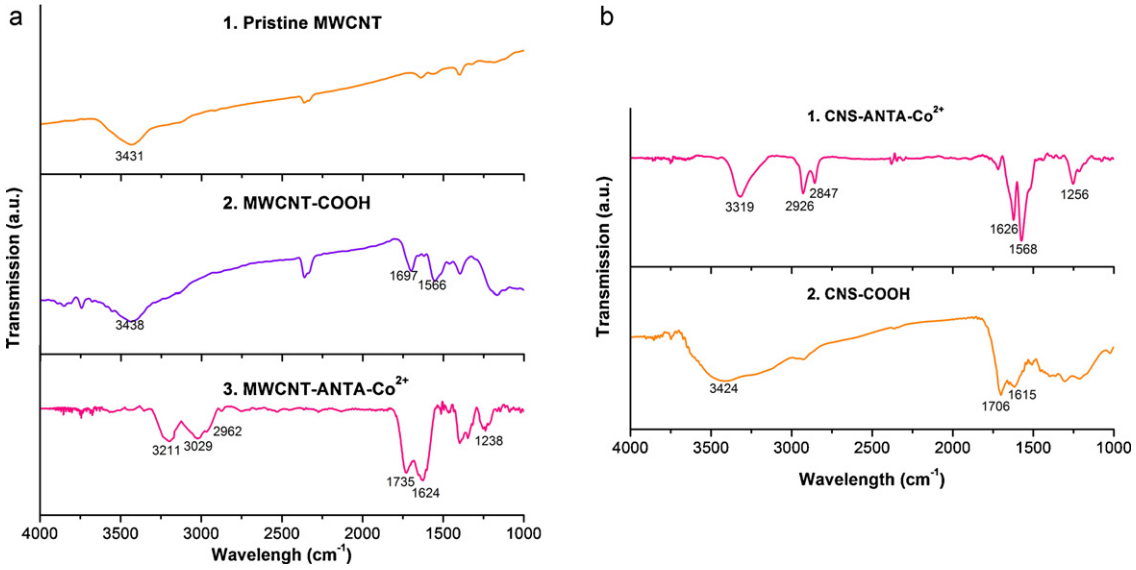

Fig. 2. FTIR spectra of the stepwise modification of MWCNTs and CNSs. (a) MWCNT modification. (1) pristine MWCNTs. (2) MWCNT–COOH. Peaks at 3438, 1697, and 1566 cm^{-1} correspond to hydroxyl groups, carboxyl groups, and carbonyl groups, respectively. (3) MWCNT–ANTA–Co^{2+} with peaks of N–H (3211 cm^{-1}), C–H (3029 and 2962 cm^{-1}), C=O (1735 and 1642 cm^{-1}) and C–O (1238 cm^{-1}). (b) CNS modification. (1) CNS–ANTA–Co^{2+} with peaks of N–H (3319 cm^{-1}), C–H (2926 and 2847 cm^{-1}), C=O (1626 and 1588 cm^{-1}) and C–O (1256 cm^{-1}). (2) CNS–COOH. Peaks at 3424, 1706, and 1615 cm^{-1} correspond to hydroxyl groups, carboxyl groups and carbonyl groups, respectively.

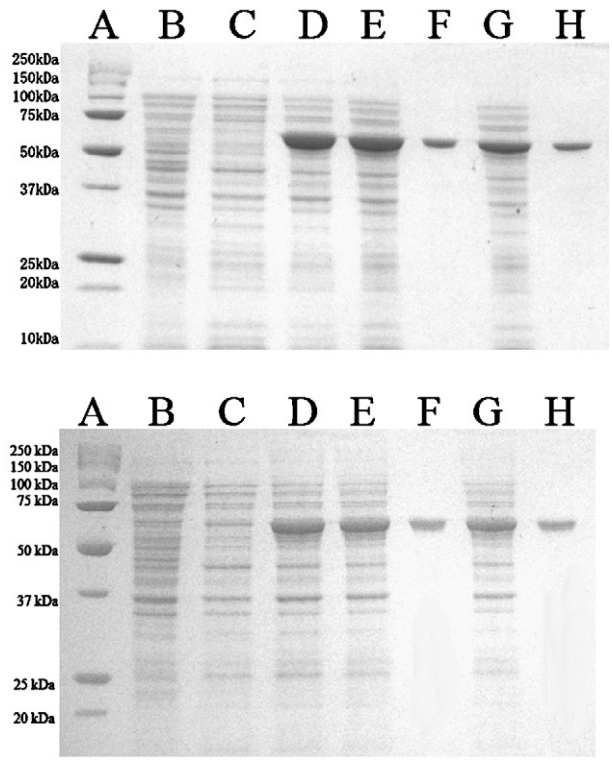

Fig. 3. SDS-PAGE of NOX overexpression and immobilization on (a) MWCNTs and (b) CNSs. Lane A: protein marker; Lane B: overnight cell culture; Lane C: uninduced; Lane D: after induction; Lane E: cell lysate; Lane F: purified NOX; Lane G: cell lysate after incubation with MWCNT/CNS–ANTA–Co^{2+} complex; Lane H: imidazole elution sample.

(NHS)-esters with ANTA–Co^{2+}. The functional chemical groups present on MWCNT–ANTA–Co^{2+} and CNS–ANTA–Co^{2+} were confirmed by FTIR. The FTIR spectra of both complexes display N–H (3200–3300 cm^{-1}), C–H (2850–3050 cm^{-1}), C=O (1550–1750 cm^{-1}) and C–O (1200–1300 cm^{-1}) peaks as expected based on their chemical structures (Fig. 2a and b). MWCNT–NOX and CNS–NOX were constructed by incubating MWCNT–ANTA–Co^{2+} and CNS–ANTA–Co^{2+} complex with cell lysate containing His-tagged NOX, respectively. In order to verify enzyme binding specificity to the functionalized nanomaterials, the bound enzymes were eluted off MWCNT–NOX and CNS–NOX with imidazole and the elution was checked using SDS-PAGE, respectively. Both eluted samples show single band on the SDS-PAGE (Fig. 3a, Lane H and b, Lane H), which suggests that immobilization is specific for both supporting materials. The enzyme loading capacity was found to be 0.196 mg enzyme/mg MWCNTs and 0.052 mg enzyme/mg CNSs, respectively. This result for modified MWCNTs is close to the published loading capacity of MWCNTs binding to enzyme covalently (0.172–0.203 mg enzyme/mg MWCNTs) [27]. We suppose that the different loading capacity between MWCNTs and CNSs is influenced by two factors: ligand density and surface area. We have calculated the ligand density of modified MWCNTs and CNSs by assuming that one His-tag coordinates with one Co^{2+} ion. The ligand density of the modified MWCNTs and CNSs is estimated to be 3.9 and 4.8×10^{11} groups/cm^2, respectively. As shown in Table 1, the surface area of MWCNTs is 280 m^2/g, which is much higher than that of CNSs (58.9 m^2/g). The modified MWCNTs have larger amount of ANTA–Co^{2+} ligands (ligand density × surface area) on their surface and hence higher loading capacity than CNSs. The surface coverage of NOX on MWCNTs and CNSs is ~49.8% and 62.8%, respectively, which implies monolayer coverage.

Table 1
Loading capacity and surface coverage comparison among different nanomaterials.

	SWCNT–NOX	MWCNT–NOX	CNS–NOX
Loading capacity (mg enzyme/mg material)	0.471	0.196	0.052
Surface area (m^2/g)	1315	280	58.9
Γ_{abs} (mg/m^2)	0.356	0.712	0.883
Ligand density ($\times 10^{11}$ groups/cm^2)	3.7	3.9	4.8
Surface coverage (%)	24.9	49.8	62.8

Table 2
Kinetic comparison between free and immobilized NOX.

Sample	K_M (μM)	V_{max} (U/mg)	k_{cat} (min^{-1})	k_{cat}/K_M (min^{-1} μM^{-1})
Free NOX[a]	53.3	27.7	1648.4	30.9
SWCNT–NOX[a]	53.4	25.7	1539.7	28.8
MWCNT–NOX	50.6	23.5	1412.3	27.9
CNS–NOX	88.7	21.5	1289.4	14.5

[a] Data obtained from [13].

3.2. Kinetic comparison

Enzyme activity retention is one of the key parameters to evaluate the immobilization process. We found that the V_{max} value of MWCNT–NOX and CNS–NOX was 23.5 U/mg and 21.5 U/mg, corresponding to 87% and 78% that of the free enzyme activity (Table 2 and Fig. 4). The controls (NOX exposed to either MWCNT–COOH or CNS–COOH) did not exhibit any activity at all, implying that non-specific enzyme adsorption is absent in either complexes. Our MWCNT–enzyme conjugate also showed better activity retention than covalently bound enzymes on MWCNTs that have activity retention between 24% and 56% [27–29]. As demonstrated in our previous work, the SWCNT–NOX conjugate could retain 92% of the native enzyme activity [13]. These findings suggest that this site-specific non-covalent immobilization procedure can be applicable to various types of carbon nanomaterials with decent retention of enzyme activity. It appears that an increase in the size of supporting material (D_{SWCNT}: 0.8–1.2 nm, D_{MWCNT}: 10–20 nm, and D_{CNS}: 741 ± 28 nm see supplementary materials Fig. S1) may lead to a

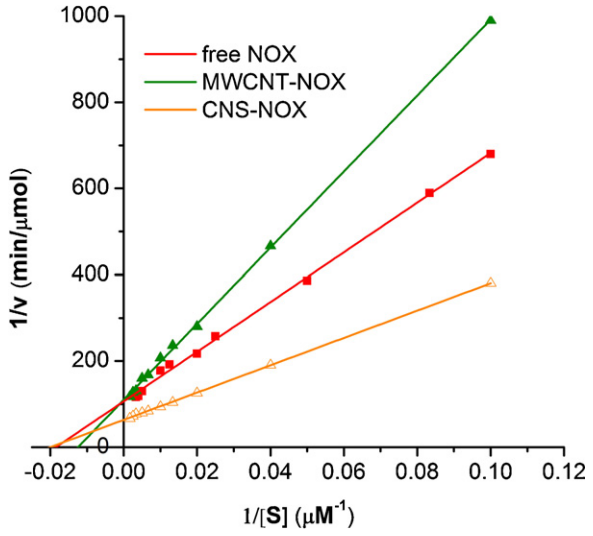

Fig. 4. Lineweaver–Burk plots obtained from free NOX (■) MWCNT–NOX (▲)and CNS–NOX (△) in air-saturated 50 mM, pH 7.0 PPB at 30 °C.

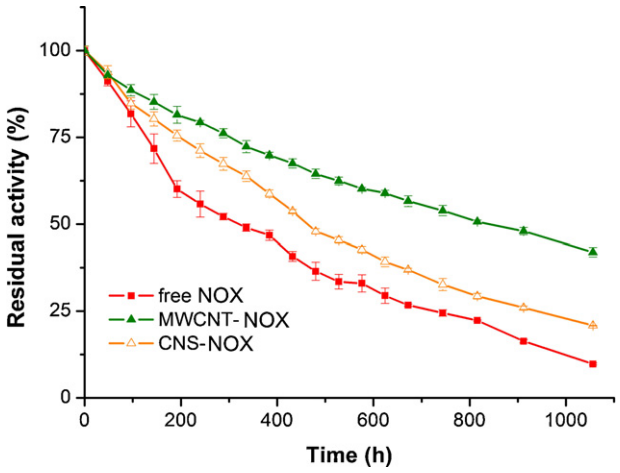

Fig. 5. Stability of free NOX (■), MWCNT–NOX (▲), and CNS–NOX (△) in 20 mM, pH 7.5 HEPES buffer at 4 °C.

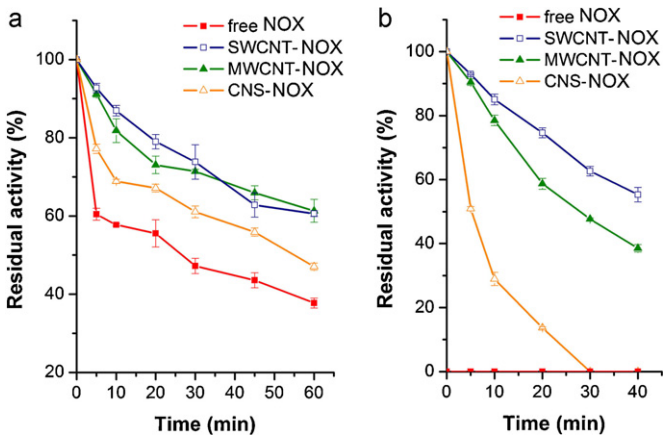

Fig. 7. Stability of free NOX (■), SWCNT–NOX (□), MWCNT–NOX (▲), and CNS–NOX (△) in 50 mM, pH 7.0 PPB at (a) 50 °C and (b) 90 °C.

decrease in V_{max}. This observation can be duly explained using the collision theory as both K_M and V_{max} are associated with the rate constant k^{coll} and hence collision frequency (Z). Since the collision frequency between the substrate molecule and the nanoparticle–catalyst system is inversely correlated to particle size (r_P), large particle size may result in low collision frequency and thus small values in both k^{coll} and V_{max}. Moreover, a decrease in particle mobility, may cause a drop in enzyme activity based on a former study on polystyrene [30]. This is probably because particle mobility is inversely proportional to r_P according to the Stokes–Einstein equation.

We also compared the NADH binding affinity among different supporting materials characterized by the K_M values of the immobilized enzymes. As shown in Table 1, CNS–NOX exhibits the highest K_M value (88.7 μM) among all of the nanoparticle–catalysts constructed in this work, implying that strong steric hindrance and diffusion limitation are present in CNS–NOX. On the other hand, the K_M values of both MWCNT–NOX (50.6 μM) and SWCNT–NOX (53.4 μM) are similar to that of native NOX (53.3 μM), suggesting negligible diffusion resistance in both cases.

3.3. Storage and thermal stability

One of the major objectives of enzyme immobilization is to improve its stability. We first examined the storage stability of both MWCNT–NOX and CNS–NOX at 4 °C over a period of ~1000 h. As revealed in Fig. 5, both immobilized enzymes exhibit better storage stability than free NOX, which is also observed in the case of SWCNT–NOX. The estimated half lives of MWCNT–NOX and CNS–NOX are around 800 h and 450 h, respectively, higher than that of free NOX (~300 h).

The temperature effect on free and immobilized NOX is displayed in Fig. 6. Enzyme immobilization on MWCNTs and CNSs results in thermal stabilization, as reflected by the elevated optimal temperature (T_{opt}) and broader active temperature range. This is consistent with our findings on SWCNT–NOX. The T_{opt} values of both MWCNT–NOX (50 °C) and CNS–NOX (60 °C) are higher than that of free NOX (37 °C). Free NOX is totally deactivated at 70 °C, whereas all types of immobilized enzymes are still active even when temperature reaches 90 °C. These results suggest that all supporting materials can help to preserve enzyme activity in a denaturing environment.

To assess the influence of different nanomaterials on thermal stability, we studied the deactivation of immobilized enzymes at 50 °C and 90 °C, with free NOX as the control. We found that all of the immobilized enzymes are more stable than native enzyme at both temperatures tested (Fig. 7). The estimated half lives ($\tau_{1/2}$) of SWCNT–NOX/MWCNT–NOX are above 90 min at 50 °C, whereas CNS–NOX is around 55 min, yet all are higher than that of the native enzyme (~25 min). At temperature of 90 °C whereby the native NOX is completely denatured, SWCNT–NOX displays the best thermal stability with the half-life of ~60 min which is double that of MWCNT–NOX (~30 min) and 12-fold higher than that of CNS–NOX (~5 min) (Fig. 7b).

We noticed that SWCNT–NOX had better stability than MWCNT–NOX and CNS–NOX. The discrepancy may be attributed to the lateral interactions between adjacent NOX molecules [31]. When enzyme surface coverage increases with enzyme concentration, the interactions between neighboring enzyme molecules also increase, which may induce change in enzyme structure and

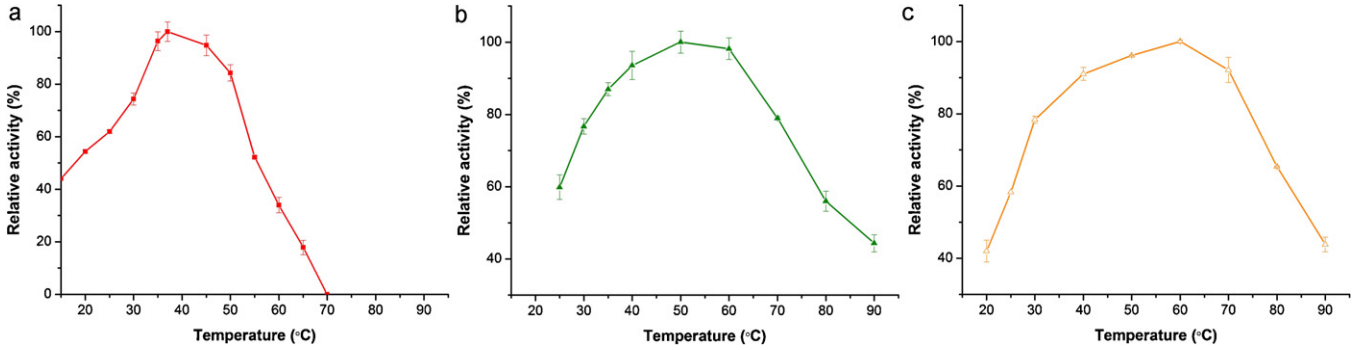

Fig. 6. Temperature profiles of (a) free NOX, (b) MWCNT–NOX, and (c) CNS–NOX. Optimum temperature: 37 °C (free NOX), 50 °C (MWCNT–NOX), and 60 °C (CNS–NOX).

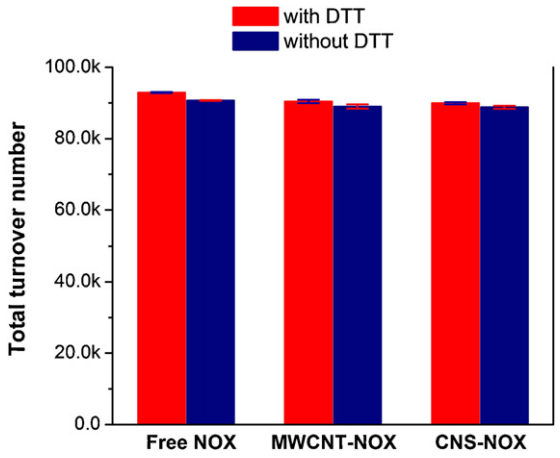

Fig. 8. Total turnover number of free NOX, MWCNT–NOX, and CNS–NOX with/without 5 mM DTT in 50 mM pH 7.0 PPB at 30 °C.

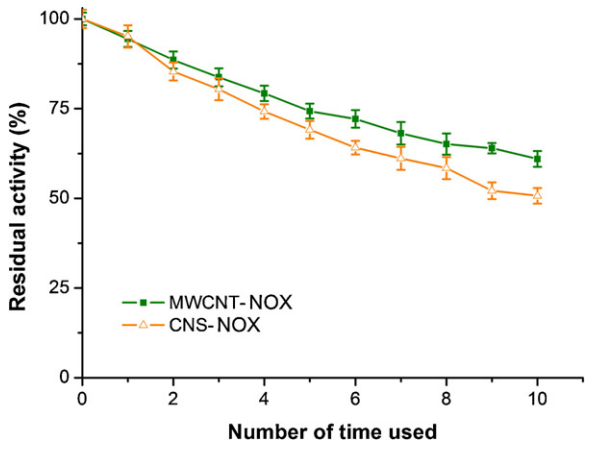

Fig. 9. Reusability of MWCNT–NOX (▲) and CNS–NOX (△).

lead to a decrease in activity [31,32]. NOX has higher surface coverage on MWCNTs and CNSs than on SWCNTs, mainly due to the larger surface area of SWCNTs (Table 1), which may in turn result in more lateral interactions occurring between neighboring NOX molecules. Moreover, lateral interactions could be suppressed by highly curved supporting materials [33]. Smaller diameters of supporting material usually imply higher surface curvature between adjacent enzyme molecules. Among these three different supporting materials, SWCNTs have the smallest diameters (0.8–1.2 nm) than MWCNTs (10–20 nm) and CNSs (741 ± 28 nm), in another word, the highest surface curvature. With a large surface area and high surface curvature, SWCNTs may have the least lateral interactions between the adjacent enzyme molecules and thus SWCNT–NOX has the best stability among all nanomaterials tested.

3.4. Operational stability

The operational stability of the native enzyme and the immobilized enzymes was found to be limited by the enzyme catalytic turnover. We evaluated the operational stability by measuring total turnover number (TTN). As illustrated in Fig. 8, the TTN values of free NOX, MWCNT–NOX and CNS–NOX are very similar to each other ($\sim 9 \times 10^4$), indicating that all have excellent operational stability and different types of supporting materials do not affect enzyme operation stability. As such, the TTN is only influenced by the enzyme itself, which is in agreement with our findings on SWCNT–NOX. Previous research on NOX from *Salmonella typhimurium* reported that the over-oxidation of the cysteine residue at the NOX active site may cause enzyme inactivation and we presumed that was also the reason for the enzyme inactivation in this case. Moreover, exogenously added reductive reagent DTT does not improve the TTN of the enzyme, probably due to a second thiol acting as a stabilizing nucleophile at the enzyme active site [34].

3.5. Reusability

Enzyme immobilization makes it feasible to reuse enzyme since it can be easily recovered from reaction medium. Fig. 9 reveals that the residual activity of immobilized NOX decreases when the recycle number increases. After ten cycles, the residual activity of MWCNT–NOX reduces to 65%, close to that of SWCNT–NOX (as shown previously), while the activity of CNS–NOX falls to 55%. The relatively rapid decline in activity of CNS–NOX may be owing to the deactivation of the densely packed NOX molecules on the surface of CNSs during batch operation [35].

4. Conclusions

Our investigations have shown that the immobilization procedure we have formerly developed with SWCNTs, which is based on the specific interaction between His-tagged enzyme and the Co^{2+} terminated nitrilotriacetate group of modified SWCNTs, can also be applied to other nanomaterials, such as MWCNTs and CNSs. Furthermore, only cell lysate, instead of pure enzyme, is required for the immobilization process. The resulting MWCNT–NOX and CNS–NOX conjugates can also retain decent enzyme activity and enhanced stability. Therefore, we believe that this method can be employed to immobilize enzyme on different carbon nanomaterials as long as they have appropriate functional groups on their surfaces. The performance of immobilized enzyme is also dependent on the properties of the supporting materials, such as size, surface area, and surface curvature.

Acknowledgement

This work was supported by Nanyang Technological University (Refs. SUG44/06 and RG124/06).

Appendix A. Supplementary data

Supplementary data associated with this article can be found, in the online version, at doi:10.1016/j.molcatb.2011.01.005.

References

[1] J.M. Broering, E.M. Hill, J.P. Hallett, C.L. Liotta, C.A. Eckert, A.S. Bommarius, Angew. Chem. Int. Ed. 45 (2006) 4670–4673.
[2] J. Kim, H.F. Jia, P. Wang, Biotechnol. Adv. 24 (2006) 296–308.
[3] E. Katz, A.F. Buckmann, I. Willner, J. Am. Chem. Soc. 123 (2001) 10752–10753.
[4] J. Kim, J.W. Grate, P. Wang, Chem. Eng. Sci. 61 (2006) 1017–1026.
[5] P. Wang, Curr. Opin. Biotechnol. 17 (2006) 574–579.
[6] H. Zhu, J. Pan, B. Hu, H.L. Yu, J.H. Xu, J. Mol. Catal. B-Enzym. 61 (2009) 174–179.
[7] J.M. Bolivar, J. Rocha-Martin, C. Mateo, F. Cava, J. Berenguer, D. Vega, R. Fernandez-Lafuente, J.M. Guisan, J. Mol. Catal. B-Enzym. 58 (2009) 158–163.
[8] P. Xue, G.Z. Lu, Y.L. Guo, Y.S. Wang, Y. Guo, J. Mol. Catal. B-Enzym. 30 (2004) 75–81.
[9] I. Aranaz, N. Acosta, A. Heras, J. Mol. Catal. B-Enzym. 58 (2009) 54–64.
[10] A.M. Klibanov, Science 219 (1983) 722–727.
[11] D.L. Falkoski, V.M. Guimaraes, M.V. de Queiroz, E.F. de Araujo, M.N. de Almeida, E.G. de Barros, S.T. Rezende, Appl. Biochem. Biotechnol. 158 (2009) 540–551.
[12] S. Hudson, J. Cooney, E. Magner, Angew. Chem. Int. Ed. 47 (2008) 8582–8594.
[13] L.A. Wang, L. Wei, Y.A. Chen, R.R. Jiang, J. Biotechnol. 150 (2010) 57–63.
[14] R.L. Hanson, M.D. Schwinden, A. Banerjee, D.B. Brzozowski, B.C. Chen, B.P. Patel, C.G. McNamee, G.A. Kodersha, D.R. Kronenthal, R.N. Patel, L.J. Szarka, Bioorg. Med. Chem. 7 (1999) 2247–2252.
[15] J. Woltinger, K. Drauz, A.S. Bommarius, Appl. Catal. A-Gen. 221 (2001) 171–185.
[16] N. Kizaki, Y. Yasohara, J. Hasegawa, M. Wada, M. Kataoka, S. Shimizu, Appl. Microbiol. Biotechnol. 55 (2001) 590–595.

[17] J.F. Chaparro-Riggers, T.A. Rogers, E. Vazquez-Figueroa, K.M. Polizzi, A.S. Bommarius, Adv. Synth. Catal. 349 (2007) 1521–1531.
[18] W. Kroutil, H. Mang, K. Edegger, K. Faber, Curr. Opin. Chem. Biol. 8 (2004) 120–126.
[19] R.R. Jiang, A.S. Bommarius, Tetrahedron Asymm. 15 (2004) 2939–2944.
[20] R.R. Jiang, B.R. Riebel, A.S. Bommarius, Adv. Synth. Catal. 347 (2005) 1139–1146.
[21] A. Jorio, G. Dresselhaus, M.S.E. Dresselhaus, Carbon Nanotubes: Advanced Topics in the Synthesis, Structure, Properties and Applications, Springer, Berlin, 2008.
[22] X.M. Sun, Y.D. Li, Angew. Chem. Int. Ed. 43 (2004) 597–601.
[23] H.S. Qian, G.F. Lin, Y.X. Zhang, P. Gunawan, R. Xu, Nanotechnology 18 (2007).
[24] P. Gunawan, R. Xu, Chem. Mater. 21 (2009) 781–783.
[25] J.M. Abad, S.F.L. Mertens, M. Pita, V.M. Fernandez, D.J. Schiffrin, J. Am. Chem. Soc. 127 (2005) 5689–5694.
[26] N. Karousis, N. Tagmatarchis, D. Tasis, Chem. Rev. 110 (2010) 5366–5397.
[27] P. Asuri, S.S. Karajanagi, E. Sellitto, D.Y. Kim, R.S. Kane, J.S. Dordick, Biotechnol. Bioeng. 95 (2006) 804–811.
[28] J.T. Cang-Rong, G. Pastorin, Nanotechnology 20 (2009).
[29] C.Z. Dinu, G. Zhu, S.S. Bale, G. Anand, P.J. Reeder, K. Sanford, G. Whited, R.S. Kane, J.S. Dordick, Adv. Funct. Mater. 20 (2010) 392–398.
[30] H.F. Jia, G.Y. Zhu, P. Wang, Biotechnol. Bioeng. 84 (2003) 406–414.
[31] A. Sethuraman, G. Vedantham, T. Imoto, T. Przybycien, G. Belfort, Proteins Struct. Funct. Bioinformat. 56 (2004) 669–678.
[32] J. Litt, C. Padala, P. Asuri, S. Vutukuru, K. Athmakuri, S. Kumar, J. Dordick, R.S. Kane, J. Am. Chem. Soc. 131 (2009) 7107–7111.
[33] P. Asuri, S.S. Karajanagi, H.C. Yang, T.J. Yim, R.S. Kane, J.S. Dordick, Langmuir 22 (2006) 5833–5836.
[34] L.B. Poole, P.A. Karplus, A. Claiborne, Annu. Rev. Pharmacol. Toxicol. 44 (2004) 325–347.
[35] Z.G. Wang, B.B. Ke, Z.K. Xu, Biotechnol. Bioeng. 97 (2007) 708–720.